Indonesian Journal of Maritime Technology (ISMATECH)
Vol. 04, Issue 01, June 2026
eISSN: 3025-518X
DOI: https://doi.org/10.35718/ismatech.v4i1.8482015

Effect of Bow and Stern Line Angle Variations on the Resistance of a 35,000 DWT Bulk Carrier Using CFD

Herawaty Magdalena Sihombing[1*], Anggra Fiveriati[1], Abdul Rohman[1], IGNA Satria Prasetya[2]

[1]Ship Manufacturing Engineering Study Program, Department of Mechanical Engineering, Politeknik Negeri Banyuwangi, Banyuwangi, Indonesia
[2]Automotive Engineering Technology Study Program, Department of Mechanical Engineering, Politeknik Negeri Banyuwangi, Banyuwangi, Indonesia

KEYWORDS
Bulk carrier;
Bow and stern line angle;
Ship resistance;
Computational Fluid Dynamics;
Holtrop method

ABSTRACT – The shipping industry requires hull designs that can reduce hydrodynamic resistance and support energy-efficient vessel operation, particularly for bulk carriers with large displacement and relatively high-power demand. This study investigates the effect of bow and stern line angle variations on the total resistance of a 35,000 DWT bulk carrier using Computational Fluid Dynamics (CFD). The CFD results were also compared with the Holtrop method and Maxsurf Holtrop estimation to assess the consistency of the total resistance prediction trend. The principal dimensions used in the hull modelling were 178 m length between perpendiculars, 185.12 m waterline length, 29.7 m breadth, 14.8 m depth, 10.3 m draft, and a service speed of 16 knots. Three hull models were analysed: Model A as the initial hull configuration with 15.4° stern line angle and 23° bow line angle, Model B with a 1° increase in both the bow and stern line angles, and Model C with a 1° decrease in both line angles. The results show that, at 16 knots, Model C produced the lowest total resistance of 647.070 kN, compared with Model A at 655.434 kN and Model B at 670.372 kN. Compared with the initial hull configuration, Model C reduced the total resistance by 8.364 kN, equivalent to approximately 1.28%. The comparison among the Holtrop method, CFD simulation, and Maxsurf Holtrop estimation showed a similar increasing trend in total resistance with ship speed, with percentage differences of 7.76% between Holtrop and CFD and 5.28% between Maxsurf Holtrop and CFD at the operational speed. Therefore, among the three tested hull model variations, Model C demonstrated the most favourable resistance performance and may contribute to reducing the effective power requirement of the 35,000 DWT bulk carrier.

*Corresponding Author | Author | ✉ (herawaty1012@gmail.com)

INTRODUCTION

The shipping industry plays a critical role in global freight transportation, particularly in transporting dry bulk commodities using bulk carrier vessels. However, large commercial ships are closely associated with high fuel consumption, propulsion power demand, and emission-related challenges. For displacement-type vessels such as bulk carriers, hydrodynamic resistance is a key factor determining the effective power required to maintain service speed. Therefore, reducing hull resistance through appropriate hull-form design is an important strategy to improve vessel energy efficiency and support more sustainable maritime operations [1], [2], [3].

Bulk carriers generally have large principal dimensions, high displacement, and relatively full hull forms to provide sufficient cargo capacity. However, these characteristics may increase hydrodynamic resistance, particularly at operational speed. Ship total resistance mainly consists of viscous resistance and wave-making resistance, both of which are strongly affected by hull geometry and flow development around the vessel [4]. Previous studies have shown that hull-form parameters, including block coefficient, hull fullness, and longitudinal geometry, can significantly influence hydrodynamic performance and resistance characteristics [5].

In ship design, resistance reduction depends on the ability of the hull form to control flow separation, pressure distribution, and wave generation. A smoother hull transition may reduce energy losses, while an unfavourable transition can increase pressure resistance and flow disturbance. Therefore, hull-form evaluation is essential in selecting an efficient ship design [6]. Several studies have also demonstrated that changes in hull geometry, design configuration, and hull-form parameters can produce different resistance responses, indicating that even small geometric modifications may influence hydrodynamic performance [7], [8], [9].

Hull geometry is commonly represented at the preliminary design stage through a lines plan, consisting of the body plan, half-breadth plan, and sheer plan. These representations define the distribution of hull sections and

control the longitudinal transition of the hull form from the bow to the stern. One geometric feature that influences this transition is the bow and stern line angle. In this study, the bow and stern line angles refer to the inclination angles of the geometric reference lines used to describe and modify the local hull-form transition in the bow entrance and stern run regions. These line angles regulate local hull-form transition without changing the vessel's principal dimensions, allowing their effect on resistance to be evaluated more directly.

The geometric transition in the bow and stern regions is important because it affects flow pattern, pressure distribution, possible flow separation, and wave formation. Computational Fluid Dynamics (CFD) provides a useful tool to evaluate these characteristics in more detail than purely empirical methods. CFD enables the analysis of velocity distribution, pressure field, streamline pattern, and resistance response around complex hull geometries [10], [11], [12]. Therefore, CFD has been widely applied in ship hydrodynamic studies, particularly for assessing the effect of hull-form variations on resistance performance [13], [14].

Previous CFD studies have investigated the hydrodynamic performance of different hull configurations and design modifications. These studies confirm that numerical simulation can compare resistance characteristics among hull forms and identify design alternatives with lower hydrodynamic resistance [16] [17] [18]. However, most previous works have focused on general hull-form modifications, bow-shape variation, stern configuration, appendage effects, or other major design parameters. Studies that specifically isolate the effect of small bow and stern line angle variations in the bow entrance and stern run regions of a 35,000 DWT bulk carrier remain limited.

Based on this research gap, this study investigates the effect of bow and stern line angle variations on the resistance of a 35,000 DWT bulk carrier using CFD simulation. Three hull configurations were evaluated: Model A as the initial hull configuration, Model B with a 1° increase in the bow and stern line angles, and Model C with a 1° decrease in the bow and stern line angles. The principal dimensions, including Lpp, Lwl, breadth, depth, draft, and service speed, were kept constant for all models so that the resistance differences could be attributed mainly to local geometric modification of the bow and stern line angles.

The CFD results were also compared with the Holtrop method and Maxsurf Holtrop estimation to assess the consistency of the resistance prediction trend, not as experimental validation. The main contribution of this study is to provide a preliminary hydrodynamic assessment of bow and stern line angle variation as a geometric consideration for reducing resistance and effective power demand in the early-stage design of a 35,000 DWT bulk carrier.

METHODS

The research methodology was conducted through several sequential stages, including problem identification, literature review, data collection, determination of the principal dimensions, lines plan development, three-dimensional hull modelling, bow and stern line angle variation, resistance analysis, comparison of resistance prediction methods, and selection of the hull configuration with the lowest resistance. In this study, the bow and stern line angles refer to the inclination angles of the straight geometric reference lines used to describe and modify the local hull-form transition in the bow entrance and stern run regions. The angle was measured relative to the horizontal baseline in the sheer or profile view of the vessel. The stern line angle represents the inclination of the hull transition line in the afterbody region, while the bow line angle represents the inclination of the hull transition line in the forebody region. These angular variations were applied locally to evaluate their influence on ship resistance without changing the principal dimensions of the vessel.

The principal dimensions of the vessel were determined using a linear regression approach based on data obtained from existing bulk carriers with characteristics similar to a 35,000 DWT vessel. The simple linear regression model is expressed as:

$$Y = a + bX \tag{1}$$

where (Y) represents the predicted principal dimension, (a) is the regression constant, (b) is the regression coefficient, and (X) is the independent variable obtained from the reference vessel database.

The resulting principal dimensions were subsequently used to develop the lines plan, consisting of the body plan, half-breadth plan, and sheer plan. The lines plan served as the geometric basis for constructing the three-dimensional hull model used in the hydrodynamic analysis.

To evaluate the influence of bow and stern line angle variations on ship resistance, three hull configurations were developed while maintaining identical principal dimensions. Model A was defined as the baseline configuration with a stern line angle of 15.4° and a bow line angle of 23°. Model B was generated by increasing both the stern and bow line angles by 1°, resulting in a stern line angle of 16.4° and a bow line angle of 24°. Conversely, Model C was generated by decreasing both the stern and bow line angles by 1°, resulting in a stern line angle of 14.4° and a bow line angle of 22°.

By maintaining the same principal dimensions for all configurations, including length, breadth, depth, draft, and service speed, the differences in hydrodynamic resistance can be attributed primarily to the local geometric modification of the bow and stern regions. The hull model variations investigated in this study are presented in Figure 1.

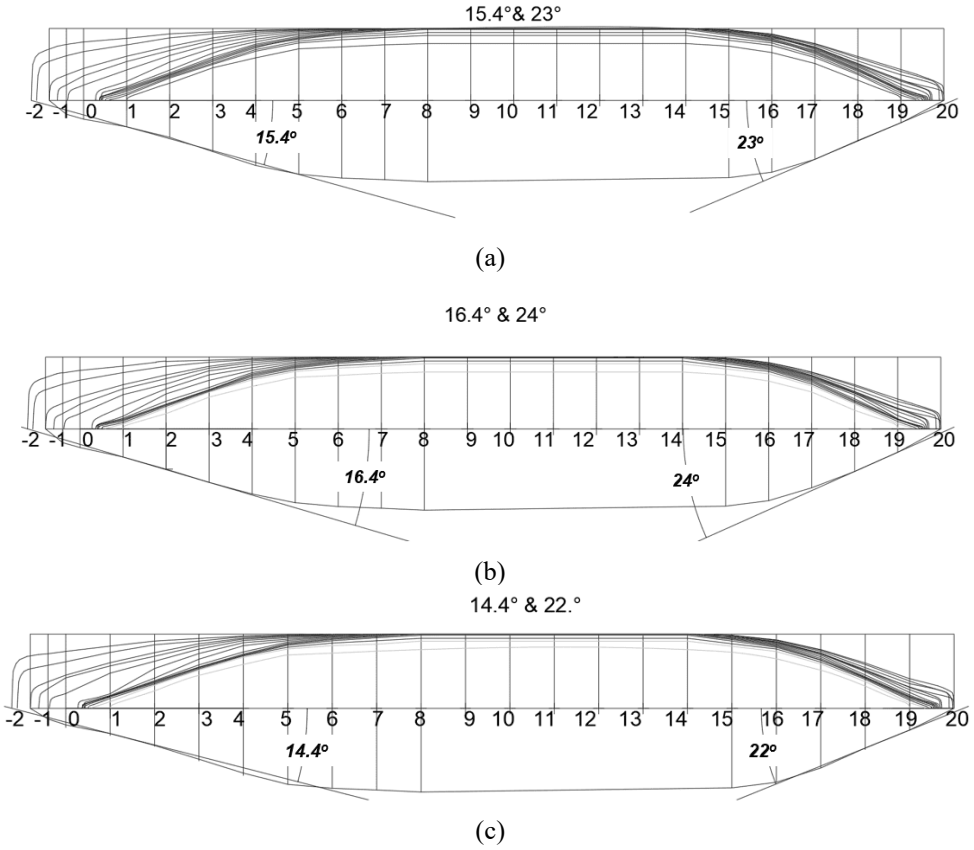

Figure 1. Hull model variations based on bow and stern line angles: (a) Model A with a 15.4° stern line angle and a 23° bow line angle, (b) Model B with a 16.4° stern line angle and a 24° bow line angle, and (c) Model C with a 14.4° stern line angle and a 22° bow line angle.

Resistance analysis was conducted using three approaches: Maxsurf Holtrop estimation, manual calculation based on the Holtrop method, and Computational Fluid Dynamics (CFD) simulation using ANSYS Fluent. Maxsurf Holtrop was used to estimate the total resistance of the vessel at different speeds, while the manual Holtrop calculation served as an empirical reference for comparison. The CFD simulation was used as the main numerical approach to evaluate the resistance and flow characteristics around each hull model.

In the CFD simulation, the three-dimensional hull model was placed inside a computational fluid domain to represent the surrounding flow region. The simulation process included the definition of boundary conditions, mesh generation, fluid property assignment, turbulence model selection, solver setup, and result evaluation. The CFD results were analyzed in terms of total resistance, streamline pattern, and flow distribution around the hull.

The resistance values obtained from CFD were then compared with the Maxsurf Holtrop estimation and manual Holtrop calculation to assess the consistency of the resistance prediction trend among the methods. This comparison was used to support the interpretation of the numerical results, not as an experimental validation. The most favourable hull configuration was selected based on the lowest total resistance and the most efficient flow characteristics among the tested models.

Computational Domain and Boundary Conditions

The CFD computational domain was developed based on the ship length to minimize boundary interference on the predicted resistance and flow field around the hull. In this study, the reference length (L) was defined as the length between perpendiculars (L_{pp} = 178) m. A half-domain approach was applied by using a symmetry plane along the longitudinal centerline of the vessel. This approach was adopted because the hull geometry and calm-

water flow condition were assumed to be symmetrical with respect to the center plane. Therefore, the half-domain model was considered sufficient to capture the main resistance trend while reducing computational cost.

The computational domain was arranged by placing the velocity inlet upstream of the bow and the pressure outlet downstream of the stern. The inlet distance was set to (1.5L) from the bow to provide sufficient flow development before reaching the hull. The outlet distance was set to (3.0L) from the stern to allow the wake region behind the hull to develop properly before reaching the outlet boundary. The outer side boundary was placed at (1.5L) from the hull region, while the top and bottom boundaries were positioned at approximately (1.0L) from the free-surface and keel regions, respectively. The computational domain and boundary condition arrangement used in this study are shown in Figure 2.

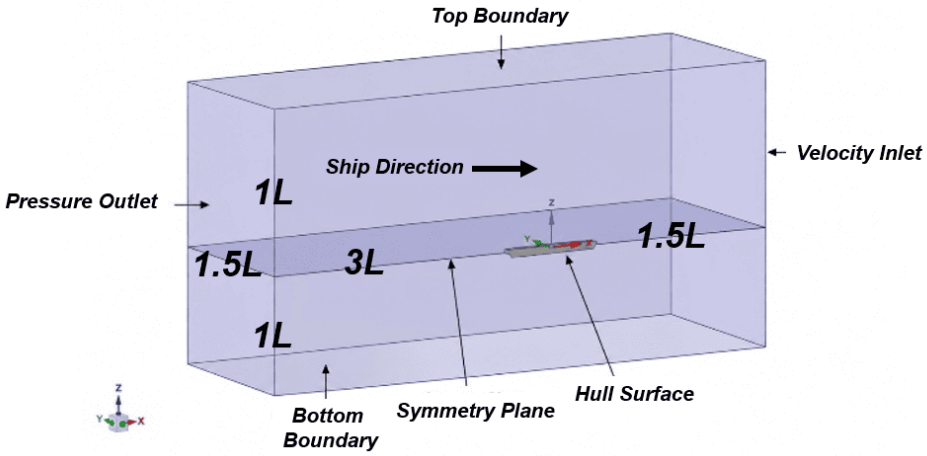

Figure 2. Computational domain and boundary conditions used in the CFD simulation.

The boundary conditions were defined based on the incoming flow direction. The upstream boundary was set as a velocity inlet, with inflow velocity adjusted to each simulated ship speed, while the downstream boundary was set as a pressure outlet to allow smooth flow exit and reduce numerical reflection. The hull surface was treated as a no-slip wall to capture viscous interaction with seawater, and the center plane was assigned as a symmetry boundary due to the half-domain model.

The outer side and bottom boundaries were defined as symmetry or free-slip boundaries to minimize blockage effects and represent open-water conditions, while the top boundary was set as an atmospheric pressure outlet. This configuration ensured adequate clearance around the hull, especially in the inlet, outlet, and wake regions, while maintaining computational efficiency.

The simulations were performed using ANSYS Fluent for ship speeds ranging from 0 to 16 knots with an interval of 2 knots. The main operating condition was evaluated at 16 knots. Seawater was used as the working fluid and was assumed to be incompressible. The computational domain was discretized using an unstructured mesh with local refinement applied around the hull surface, bow, stern, and free-surface regions to improve the accuracy of resistance prediction. A pressure-based steady-state solver was employed, and the free surface was modelled using the Volume of Fluid (VOF) approach to capture the air–water interface. The k–ω SST turbulence model was selected due to its capability in predicting near-wall flow behaviour and adverse pressure gradient effects around ship hulls.

Convergence was assessed based on the reduction of residuals and the stabilization of the total resistance value during the iterative process. The residual convergence criterion was set to 1×10^{-5} for governing equations. The simulation outputs analysed in this study included total resistance, residual convergence history, and flow-field characteristics for each hull model variation.

Based on Figure 2, the computational domain was modeled using a half-domain approach with a symmetry plane along the vessel centerline. The upstream and downstream boundaries were set as a velocity inlet and pressure outlet, respectively, while the hull surface was defined as a no-slip wall to capture viscous interaction with seawater. The outer side and bottom boundaries were treated as symmetry or free-slip boundaries to reduce blockage effects, and the top boundary was set as an atmospheric pressure outlet. These boundary conditions were applied to obtain the flow distribution and total resistance for each hull variation.

Resistance Prediction Method

The ship resistance prediction was conducted to obtain the total resistance acting on the hull and to compare the resistance trend obtained from different prediction approaches. In this study, three approaches were used:

manual calculation based on the Holtrop method, resistance estimation using Maxsurf Holtrop, and Computational Fluid Dynamics (CFD) simulation using ANSYS Fluent. The CFD simulation was used as the main numerical approach to evaluate the resistance and flow characteristics of each hull model, while the Holtrop method and Maxsurf Holtrop estimation were used as comparative methods to assess the consistency of the resistance prediction trend.

The manual calculation was carried out using the Holtrop method, which estimates ship resistance based on empirical formulations and hull-form parameters. The calculation includes the estimation of frictional resistance and residuary resistance, with corrections related to the hull-form characteristics. The frictional resistance coefficient was calculated using the ITTC 1957 friction line. Before calculating the frictional resistance coefficient, the Reynolds number was determined using the following equation:

$$R_n = (V \times L_{wl}) / \nu \tag{2}$$

where R_n is the Reynolds number, V is the speed of the ship, L_{wl} is the length of the ship's waterline, and ν is the kinematic viscosity of the fluid.

After the Reynolds number was obtained, the frictional resistance coefficient was calculated using the ITTC 1957 equation as follows:

$$CF = 0{,}075 / (log10\, R_n - 2)^2 \tag{3}$$

where CF is the coefficient of friction resistance. Furthermore, the friction resistance of the ship is calculated using the equation:

$$RF = 0{,}5 \times \rho \times CF \times S \times V^2 \tag{4}$$

where RF is the frictional resistance, ρ is the density of seawater, S is the wetted surface area of the hull, and V is the ship speed. Friction resistance is used to determine the magnitude of the resistance that arises due to the interaction between the wet surface of the hull and fluids.

In addition to frictional resistance, the Holtrop method also accounts for residuary resistance, which is influenced by hull geometry, displacement, Froude number, and the longitudinal distribution of hull volume. The Froude number was calculated using the following equation:

$$F_n = \frac{V}{\sqrt{g \times L_{wl}}} \tag{5}$$

where F_n is the Froude number, V is the speed of the ship, g is the acceleration of gravity, and L_{wl} is the length of the ship's waterline. The Froude number value is used to see the relationship between the speed of the ship and the characteristics of wave formation around the hull.

Maxsurf Holtrop was used to estimate the total resistance of the hull at several speed variations. The Maxsurf results were compared with the manual Holtrop calculation and CFD simulation results to evaluate the consistency of the resistance trend among the methods. Meanwhile, the CFD simulation was conducted by placing the three-dimensional hull model inside the computational fluid domain, defining the boundary conditions, generating the computational mesh, selecting the fluid and turbulence models, running the solver, and evaluating the resulting resistance and flow field.

The comparison among the Holtrop method, Maxsurf Holtrop estimation, and CFD simulation was performed using the percentage difference. This value was used to indicate the magnitude and direction of the difference between two resistance prediction methods. A positive value indicates that the first method produces a higher resistance value than the reference method, while a negative value indicates that the first method produces a lower resistance value than the reference method. The percentage difference was calculated using the following equation:

$$Precentage\ Difference\ (\%) = \left({}^{(R1 - R2)}/_{R2}\right) \times 100\% \tag{6}$$

where $R1$ and $R2$ are the resistance values of the two methods compared. The percentage difference was used to evaluate the consistency of the predicted resistance trends obtained from the calculation and simulation results.

The most favourable tested configuration was determined based on the lowest total resistance value, the consistency of the resistance trend among the prediction methods, and the stability of the CFD convergence history.

RESULTS AND DISCUSSION

Principal Dimensions of the Vessel

The first stage of the results analysis was the determination of the principal dimensions of the vessel, which served as the basis for hull modelling. These dimensions were used as the main reference for developing the lines plan, constructing the three-dimensional hull model, and conducting the total resistance analysis for each bow and stern line angle variation. The principal dimensions and hull coefficients of the 35,000 DWT bulk carrier used in this study are presented in Table 1.

Table 1. Principal dimensions of the 35,000 DWT bulk carrier.

Main Data of Bulk Carriers 35,000 DWT			
No	Item	Size	Units
1	L_{pp} (Length Between Perpendiculars)	178	Meters
2	L_{wl} (Length at Waterline)	185.12	Meters
3	L_{disp} (Length of Displacement)	181.56	Meters
4	B (Breadth)	29.7	Meters
5	H (Height / Depth)	14.8	Meters
6	T (Draft)	10.3	Meters
7	V_S (Vessel Speed)	16	Knot
8	C_b (Block Coefficient)	0.7420	-
9	C_p (Prismatic Coefficient)	0.752	-
10	C_m (Midship Coefficient)	0.987	-
11	L_{cb} (Longitudinal center of buoyancy)	3.359	%
12	Mass Displacement	42,241.72	Tonnes
13	C_{wp} (Waterplane Coefficient)	0.806	-

Table 1 presents the principal dimensions and hull coefficients of the 35,000 DWT bulk carrier used as the basis for hull modelling and total resistance analysis. The vessel has an L_{pp} of 178 m, an L_{wl} of 185.12 m, a breadth of 29.7 m, a depth of 14.8 m, a draft of 10.3 m, and a service speed of 16 knots. The block coefficient of 0.7420 indicates that the vessel has a relatively full hull form, which is consistent with the general characteristics of bulk carrier vessels. The displacement of 42,241.72 tonnes represents the vessel displacement obtained from the hull geometry calculation. These principal dimensions and hull coefficients were then used as the basis for developing the initial hull model, and the bow and stern line angle variations were analyzed in this study.

After the principal dimensions were determined, the initial hull geometry was represented through a lines plan. The lines plan was presented separately to provide a clearer description of the hull form, including the body plan and sheer plan. The body plan illustrates the hull cross-sections at each station, while the sheer plan shows the vessel's longitudinal profile from the side view. These drawings served as the geometric basis for developing the three-dimensional hull model and the bow and stern line angle variations.

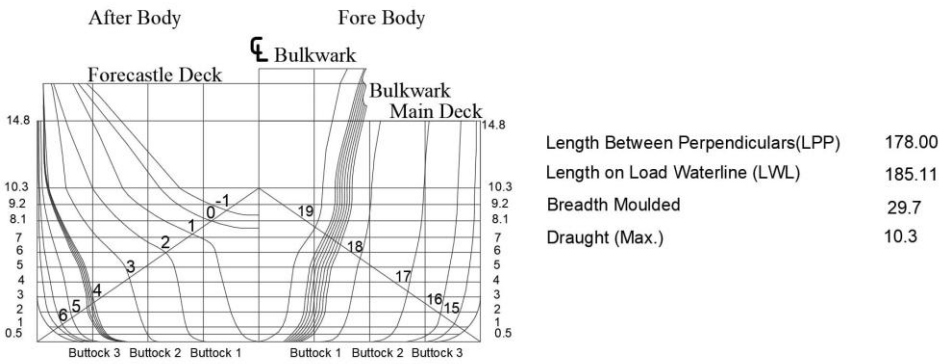

Figure 3. Body plan of the 35,000 DWT bulk carrier.

Based on Figure 3, the body plan shows the hull cross-sectional shapes at each station, from the bow to the stern. This drawing helps assess the proportionality and continuity of the hull sections along the vessel length. It also serves as the sectional basis for constructing the three-dimensional hull model used in the total resistance analysis.

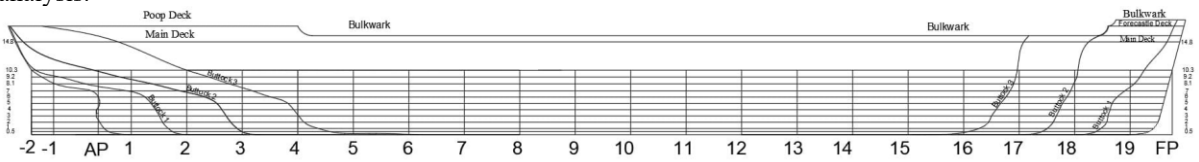

Figure 4. Sheer plan of the 35,000 DWT bulk carrier.

Based on Figure 4, the sheer plan shows the vessel's longitudinal profile from the side view, including the baseline, deck line, and hull-form transition from bow to stern. It was used to evaluate the hull's longitudinal geometry and to guide the development of bow and stern line angle variations, especially in the bow entrance and stern run regions. Since the principal dimensions were kept constant, differences in total resistance can be mainly attributed to local geometric changes in the bow and stern areas.

Thus, the body plan and sheer plan play an important role as the geometric basis for constructing the three-dimensional hull models. These drawings also provide the reference geometry for evaluating the resistance characteristics of each hull variation using Maxsurf Holtrop estimation, manual Holtrop calculation, and CFD simulation.

Mesh Sensitivity Analysis

The mesh independence test was performed to ensure that the total resistance values obtained from the CFD simulations were not significantly affected by the number of cells used in the computational domain. This step is important because the total resistance difference between Model C and Model A at the operating speed is relatively small, approximately 1.28%. Therefore, it is necessary to ensure that the observed total resistance difference is mainly caused by hull geometry variation rather than mesh density or numerical instability.

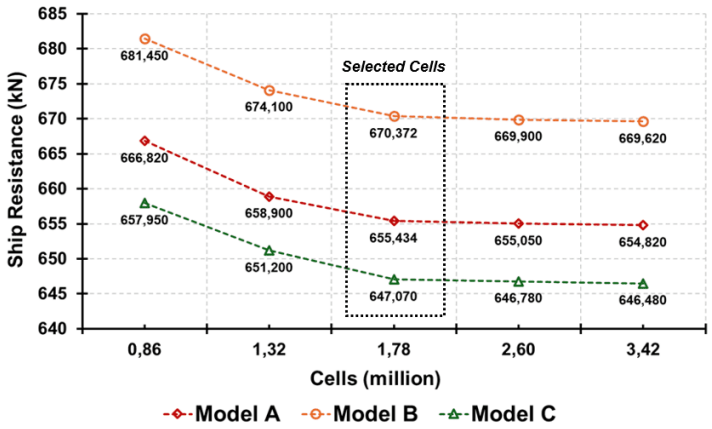

Figure 5. Mesh independence test of hull model variations at 16 knots.

Based on Figure 5, the mesh independence test was conducted using five mesh densities: 0.86 million, 1.32 million, 1.78 million, 2.60 million, and 3.42 million cells. The results show that the total resistance values change noticeably from 0.86 million to 1.32 million cells. However, after the mesh density reaches 1.78 million cells, the change in total resistance becomes relatively small for all hull model variations.

At 1.78 million cells, the total resistance values were 655.434 kN for Model A, 670.372 kN for Model B, and 647.070 kN for Model C. These values are very close to those obtained using the finest mesh of 3.42 million cells, where the total resistance values were 654.820 kN for Model A, 669.620 kN for Model B, and 646.480 kN for Model C. The percentage differences between the selected mesh and the finest mesh were approximately 0.094% for Model A, 0.112% for Model B, and 0.091% for Model C.

The small differences indicate that the solution had reached a stable mesh-independent trend at 1.78 million cells. Therefore, the mesh with 1.78 million cells was selected for the main CFD simulations because it provides a reasonable balance between numerical accuracy and computational efficiency. By using this selected mesh, the

total resistance comparison among Model A, Model B, and Model C can be considered more representative of the effect of bow and stern line angle variations, rather than being dominated by the influence of mesh density.

Comparison of Holtrop, CFD, and Holtrop Maxsurf Results

In addition to evaluating the total resistance of each hull model variation, this study also assessed the consistency of the total resistance prediction trend obtained from three different approaches: the Holtrop method, CFD simulation, and Maxsurf Holtrop estimation. The Holtrop method was used as an empirical total resistance prediction approach based on hull-form parameters and resistance coefficients. Maxsurf Holtrop was used as a software-based estimation method, while CFD simulation was used as the main numerical approach to evaluate the flow field and total resistance around the hull.

The comparison among these three approaches was conducted to examine whether the CFD results showed a reasonable total resistance trend relative to the empirical and software-based prediction methods. This comparison is important because each method uses different assumptions and calculation procedures. The Holtrop method and Maxsurf Holtrop estimation rely on empirical formulations and hull-form coefficients, while CFD calculates the flow characteristics around the hull based on the computational domain, mesh resolution, boundary conditions, turbulence model, and hull geometry. Therefore, differences in total resistance values among the methods are expected, especially at higher speeds where wave-making effects and pressure distribution become more influential.

The tolerance limits used in this study were adopted from previous studies as reference values for assessing the consistency among the total resistance prediction methods. The tolerance limit was set at 10% for the comparison between the Holtrop method and Maxsurf Holtrop estimation [19], 13% for the comparison between the Holtrop method and CFD simulation [20], and 5% for the comparison between Maxsurf Holtrop estimation and CFD simulation [21]. These limits were used to evaluate the level of agreement among the methods, not as experimental validation. A complete validation would require experimental data, such as towing tank measurements or full-scale sea trial results.

Table 2 shows that the total resistance obtained from the three methods increases as the ship speed increases. This trend is consistent with the general behaviour of ship resistance, where higher speed leads to greater hydrodynamic resistance acting on the hull. At low speeds, the differences among the methods are relatively small. However, the deviation becomes more noticeable at medium to high speeds because the contribution of wave-making resistance, pressure distribution, and hull-form effects becomes more significant.

Table 2. Comparison of total resistance and percentage difference between Holtrop, CFD, and Maxsurf methods.

Speed	Holtrop Total Resistance	CFD Total Resistance	Holtrop Maxsurf Total Resistance	Difference Holtrop & Holtrop Maxsurf	Holtrop & CFD Difference	Difference Holtrop Maxsurf & CFD	Tolerance Limits of Holtrop & Holtrop Maxsurf	Holtrop Tolerance Limits & CFD	Holtrop Maxsurf & CFD Tolerance Limits
(Knots)	(kN)	(kN)	(kN)	(%)	(%)	(%)	(%)	(%)	(%)
0	0.0089420	0	0	0%	0%	0%			
2	12.9314832	12.124	12.54064	-3.02%	6.66%	-3.32%			
4	48.6040382	45.786	46.12941	-5.09%	6.15%	-0.74%			
6	105.0264317	97.152	98.42931	-6.28%	8.11%	-1.30%			
8	180.8338935	175.498	167.93359	-7.13%	3.04%	4.50%	10.00%	13.00%	5.00%
10	275.0128147	270.516	254.06160	-7.62%	1.66%	6.48%			
12	388.0428901	385.362	360.03983	-7.22%	0.70%	7.03%			
14	525.2891919	520.290	497.96686	-5.20%	0.96%	4.48%			
16	706.2693263	655.434	691.98580	-2.02%	7.76%	-5.28%			

The comparison between CFD, Holtrop, and Maxsurf Holtrop results was conducted to evaluate the consistency of the predicted resistance trends among different calculation approaches. This comparison should not be interpreted as a full experimental validation, since no towing-tank or full-scale measurement data were available. Instead, it serves as a supplementary assessment of the reliability and consistency of the numerical predictions.

At the operational speed of 16 knots, the Holtrop method produced a total resistance of 706.269 kN, while the CFD simulation produced 655.434 kN. The Maxsurf Holtrop estimation produced a total resistance of 691.986 kN. The percentage difference between the Holtrop method and CFD simulation was 7.76%, which is still within the 13% tolerance limit adopted in this study. Meanwhile, the percentage difference between Maxsurf Holtrop and CFD was 5.28% in magnitude, which slightly exceeds the 5% tolerance limit. Similar exceedances can also

be observed at 10 knots and 12 knots, where the difference between Maxsurf Holtrop and CFD is greater than the adopted 5% limit.

These differences indicate that the three methods do not produce identical total resistance values. This condition is reasonable because the Holtrop method and Maxsurf Holtrop estimation are based on empirical or semi-empirical formulations, while CFD simulation resolves the flow field numerically. In CFD, the total resistance value is influenced by the computational domain, mesh quality, boundary conditions, turbulence model, and the detailed hull geometry. In contrast, the Holtrop method simplifies the hull-resistance relationship through empirical coefficients and hull-form correction factors. Therefore, some deviation among the methods is expected.

Although some percentage differences exceed the adopted tolerance limit, the three methods still show a similar increasing total resistance trend with increasing ship speed. This indicates that the CFD simulation results remain consistent with the general total resistance trend predicted by the empirical and software-based methods. Therefore, the comparison among Holtrop, CFD, and Maxsurf Holtrop is used in this study as a method-consistency assessment, not as experimental validation. The main evaluation of the hull model variations was based on the CFD total resistance results and the flow characteristics of each hull model.

A graphical comparison of the total resistance obtained from the three methods is presented in Figure 6. The graph was used to provide a clearer visualization of the resistance trend over the speed range from 0 to 16 knots.

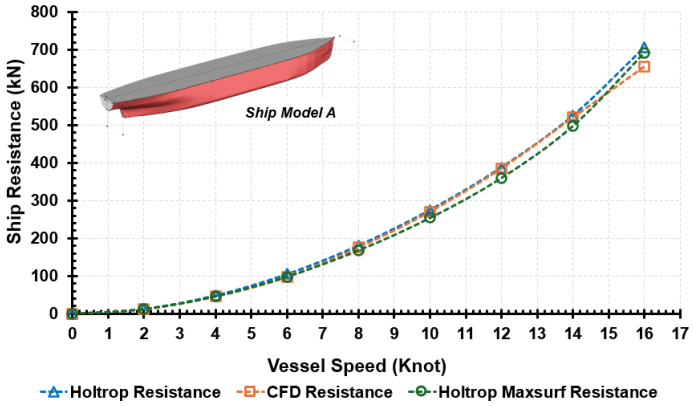

Figure 6. Comparison of total resistance obtained from the Holtrop method, CFD simulation, and Maxsurf Holtrop estimation.

Based on Figure 6, the three methods show a relatively similar trend, where the total resistance increases with ship speed. The increase becomes more pronounced at medium to high speeds, indicating the stronger influence of hydrodynamic effects as the vessel approaches its operational speed. In general, the Holtrop method gives the highest total resistance values, while CFD gives lower values at the operational speed. Maxsurf Holtrop produces resistance values that are generally between those of the Holtrop method and CFD at 16 knots.

At 16 knots, the total resistance obtained from the Holtrop method was 706.269 kN, compared with 655.434 kN from CFD and 691.986 kN from Maxsurf Holtrop. This difference reflects the different nature of the prediction approaches. The Holtrop method and Maxsurf Holtrop rely on empirical hull-form relationships, while CFD calculates the resistance from the numerical solution of the flow around the hull. Therefore, the comparison in Figure 6 supports the interpretation that the CFD results follow a reasonable resistance trend and can be used as the basis for evaluating the resistance performance of the three hull model variations.

Resistance Comparison of Hull Model Variations

Using the principal dimensions and hull geometry presented in the previous section, resistance analysis was conducted for three hull model variations, namely Model A, Model B, and Model C. Model A represent the initial hull configuration with a stern line angle of 15.4° and a bow line angle of 23°. Model B represents the modified configuration with a 1° increase in both the bow and stern line angles, resulting in a stern line angle of 16.4° and a bow line angle of 24°. Meanwhile, Model C represents the modified configuration with a 1° decrease in both the bow and stern line angles, resulting in a stern line angle of 14.4° and a bow line angle of 22°.

All three models were developed using the same principal dimensions so that the total resistance differences could be attributed mainly to the variation in the bow and stern line angles. The CFD simulations were carried out at ship speeds ranging from 0 to 16 knots with an interval of 2 knots. This speed range was used to evaluate the resistance trend of each hull model and to identify the influence of bow and stern line angle variation on the total resistance. The comparison of total resistance for each hull model variation is presented in Table 3.

Table 3. CFD-based total resistance comparison of the hull model variations.

Speed	Model A (15.4° & 23°)	Model B (16.4° & 24°)	Model C (14.4° & 22°)
(Knots)	Total Resistance (kN)	Total Resistance (kN)	Total Resistance (kN)
0	0	0	0
2	12.124	12.169	11.850
4	45.786	46.350	45.244
6	97.152	101.652	99.262
8	175.498	177.622	173.476
10	270.516	273.842	267.514
12	385.362	390.218	381.288
14	520.290	526.578	516.156
16	655.434	670.372	647.070

Based on Table 3, the total resistance of all hull models increases as the ship speed increases. At lower speeds, the total resistance differences among the three models are relatively small. However, the differences become more apparent at higher speeds, particularly near the operational speed of 16 knots. At 16 knots, Model A produced a total resistance of 655.434 kN, Model B produced 670.372 kN, and Model C produced 647.070 kN. These results show that Model C generated the lowest resistance among the three tested configurations.

Compared with Model A as the initial hull configuration, Model B increased the total resistance by 14.938 kN, equivalent to approximately 2.28%. In contrast, Model C reduced the total resistance by 8.364 kN, equivalent to approximately 1.28% compared with Model A. This result indicates that the variation of the bow and stern line angles influences the hydrodynamic resistance of the hull. Increasing the stern line angles by 1° in Model B resulted in higher total resistance, whereas reducing the stern line angles by 1° in Model C produced the lowest total resistance at the operational speed.

To provide a clearer comparison of the operational speed, the total resistance values of Model A, Model B, and Model C at 16 knots are presented as a bar chart in Figure 7. This figure highlights the total resistance difference among the tested hull configurations and identifies the model with the highest and lowest total resistance more directly.

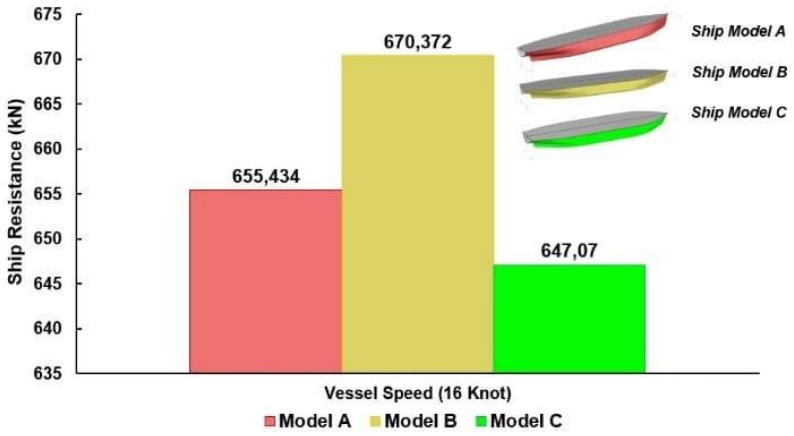

Figure 7. Total resistance comparison of hull model variations at 16 knots.

Based on Figure 7, Model B produced the highest total resistance at 16 knots, with a value of 670.372 kN. Model A, as the initial hull configuration, produced a total resistance of 655.434 kN, while Model C produced the lowest total resistance of 647.070 kN. Compared with Model A, Model C reduced the total resistance by 8.364 kN, equivalent to approximately 1.28%. In contrast, Model B increased the total resistance by 14.938 kN, equivalent to approximately 2.28% compared with Model A.

These results indicate that a 1° reduction in the bow and stern line angles may contribute to a moderate decrease in total resistance, while a 1° increase in the stern line angles tends to increase total resistance. Therefore, Figure 7 confirms that stern line angle variation affects the total resistance of the vessel. However, the magnitude of the total resistance reduction in Model C should be interpreted proportionally, as the improvement relative to the initial model remains moderate.

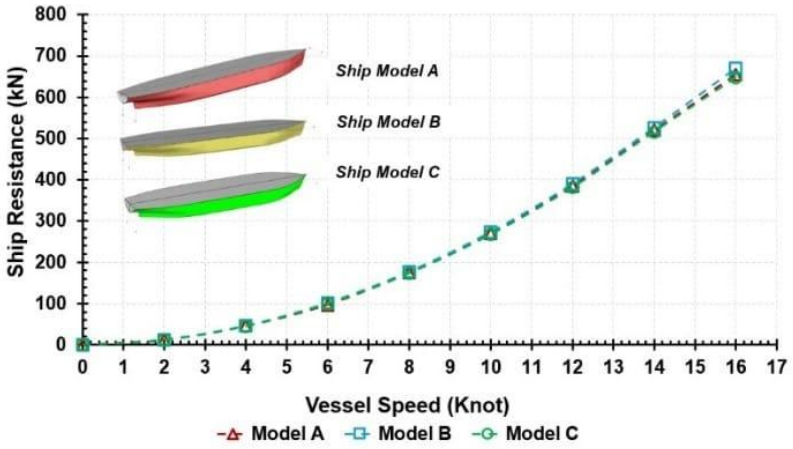

Figure 8. Total resistance comparison of hull model variations.

Based on Figure 8, all hull models show an increasing trend in total resistance as ship speed rises, indicating that the bow and stern line angle variations do not alter the general speed–resistance relationship. At low speeds, the resistance differences among the models are relatively small because the flow is less sensitive to minor local hull-form changes, and frictional resistance remains dominant.

As the speed increases, especially toward 16 knots, the influence of hull-form variation becomes more evident. Higher flow energy around the bow and stern makes the pressure distribution, streamline pattern, and wave-making characteristics more sensitive to changes in the hull transition. The wider separation among the resistance curves indicates that bow and stern line angle variations have a greater effect under higher hydrodynamic loads.

Model B, with a 1° increase in bow and stern line angles, produces the highest total resistance, possibly due to less favorable flow transition and increased pressure resistance. In contrast, Model C, with a 1° reduction in the line angles, shows the lowest resistance, suggesting a smoother hull-form transition for the tested configuration. This interpretation can be strengthened by flow visualization results, such as streamlines, velocity, or pressure contours, to explain the physical mechanisms behind the resistance differences.

At 16 knots, Model C reduces the total resistance by approximately 1.28% compared with Model A. Therefore, the result should be interpreted as a moderate improvement in hydrodynamic performance rather than a major reduction in resistance. Overall, Figure 8 supports the results presented in Table 3, showing that bow and stern line angle variation affects the resistance performance of the vessel, particularly at higher speeds where pressure distribution, flow development, and wave-making effects become more influential.

Flow Characteristics around the Hull

Streamline and velocity-contour analyses were performed to examine the flow characteristics around each hull model at the operational speed of 16 knots. This visualization was used to identify the flow pattern, the level of flow regularity, and the possible flow disturbance caused by changes in the bow and stern line angles. Since the three hull models have the same principal dimensions, the difference in flow characteristics can be associated mainly with the local geometric changes in the bow entrance and stern run regions. The streamline and velocity-contour visualization of the three hull models is shown in Figure 9.

Based on Figure 9, the three hull models show different flow characteristics around the hull at 16 knots. In Model A, the streamline pattern follows the initial hull geometry with a relatively regular flow distribution along the side of the hull. This condition represents the baseline flow behaviour of the initial model. The velocity contour also shows flow acceleration around the bow entrance and along the hull side, which is expected because the incoming flow interacts directly with the hull surface at operational speed.

In Model B, the flow pattern appears more disturbed and more widely distributed around the hull, particularly from the bow entrance toward the midship region. The velocity contour indicates a more pronounced flow acceleration around the hull side. This condition may indicate a less favourable hull-form transition caused by the 1° increase in the bow and stern line angles. At higher speeds, this geometric change can increase the sensitivity of the flow to local curvature, resulting in stronger changes in velocity distribution and pressure development around the hull. This explains why the total resistance difference between Model B and the other models becomes more visible at high speed, especially at 16 knots. The flow behaviour shown in Figure 9(b) is consistent with the total resistance result, where Model B produced the highest total resistance among the tested configurations.

In contrast, Model C shows a more controlled streamline pattern along the hull. The flow appears to follow the hull contour more smoothly compared with Model B, particularly in the transition from the bow region toward

the midship section. This suggests that the 1° reduction in the bow and stern line angles may improve the local hull-form transition and reduce flow disturbance around the hull. The smoother streamline development in Model C supports its lower total resistance at 16 knots compared with Model A and Model B.

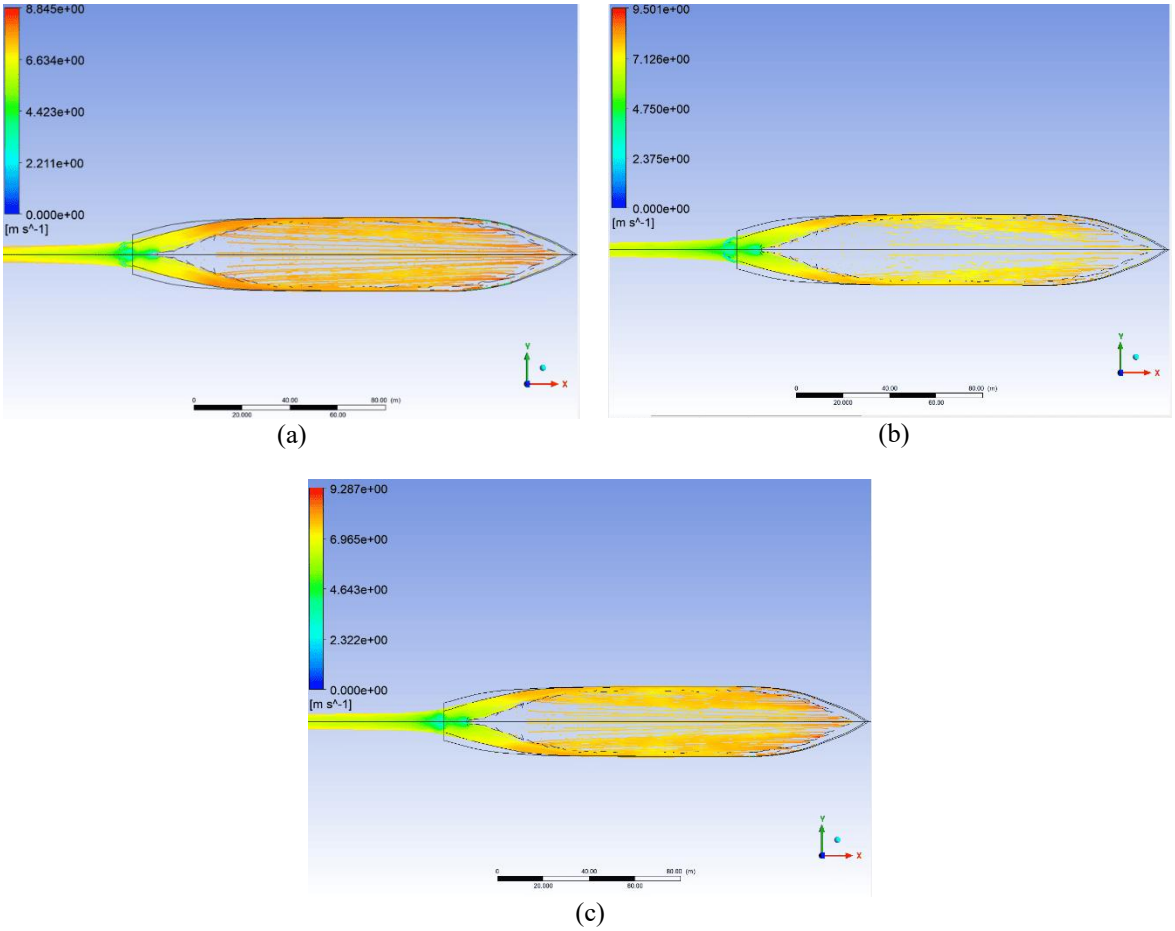

Figure 9. Streamline and velocity-contour visualization of the hull model variations: (a) Model A, (b) Model B, and (c) Model C.

The reason why the effect of bow and stern line angle variation becomes clearer at higher speeds is related to the increase in hydrodynamic sensitivity. At lower speeds, the flow around the hull is less energetic, and the total resistance difference caused by small geometric variations remains relatively small. Under this condition, the influence of local bow and stern line-angle changes on velocity distribution and pressure development is not yet dominant. However, at higher speeds, the dynamic pressure and flow acceleration around the hull increase. As a result, small changes in hull-form transition can produce a more noticeable difference in streamline pattern, velocity contour, and resistance response.

Therefore, Figure 9 helps explain the trend shown in Figure 8. The total resistance curves begin to separate more clearly at higher speeds because the flow field becomes more sensitive to the geometry of the bow and stern regions. Model B, with a larger stern line angle, tends to generate a less favourable flow distribution and produces the highest total resistance. Meanwhile, Model C, with a smaller stern line angle, shows a more stable streamline pattern and produces the lowest total resistance. Although pressure contours are not presented separately in this study, the streamline and velocity-contour visualization provides supporting evidence that the difference in resistance at 16 knots is related to changes in flow behaviour around the hull.

Evaluation of Hull Model Variations

The evaluation of hull model variations was carried out based on the CFD resistance results, flow characteristics, and the consistency of the resistance trend obtained from the comparative methods. In this study, all hull models were developed using the same principal dimensions, namely an L_{pp} of 178 m, an L_{wl} of 185.12 m, a breadth of 29.7 m, a depth of 14.8 m, a draft of 10.3 m, and a service speed of 16 knots. Therefore, the difference in total resistance among the models was not caused by changes in the main dimensions of the vessel, but was

mainly associated with the local geometric modification introduced through the bow and stern line angle variations.

The bow and stern line angle variations influenced the geometric transition of the hull form, particularly in the bow entrance and stern run regions. Although the principal dimensions remained unchanged, these angular modifications affected the sectional shape and longitudinal hull representation, as reflected in the body plan and sheer plan. As a result, relatively small changes in the hull-form geometry altered the flow development around the vessel and produced measurable differences in total resistance performance. This finding highlights that modifications to the bow and stern line angles can affect hydrodynamic performance without altering the overall principal dimensions of the ship.

Based on the CFD results at the operational speed of 16 knots, Model C produced the lowest total resistance of 647.070 kN. This value is lower than that of Model A, which produced 655.434 kN, and Model B, which produced 670.372 kN. Compared with Model A as the initial configuration, Model C reduced the total resistance by 8.364 kN, equivalent to approximately 1.28%. In contrast, Model B increased the total resistance by 14.938 kN, or approximately 2.28%, compared with Model A. Model C also produced 23.302 kN lower total resistance than Model B, equivalent to approximately 3.48%. Therefore, among the three configurations investigated, Model C demonstrated the most favourable total resistance performance. However, this conclusion is limited to the specific bow and stern line angle variations examined in the present study and should not be interpreted as indicating the overall optimum hull form.

These results indicate that reducing the bow and stern line angles by 1° produced a more favourable resistance response among the tested configurations. The lower total resistance of Model C is also supported by the streamline and velocity-contour visualization, which showed a more controlled flow pattern around the hull at 16 knots. In contrast, Model B tended to produce a less favourable flow distribution and the highest total resistance among the three models. This suggests that the local hull-form transition caused by bow and stern line angle variation can influence the hydrodynamic behaviour of the vessel, especially at operational speed.

The comparison among the Holtrop method, CFD simulation, and Maxsurf Holtrop estimation also showed a similar increasing resistance trend with ship speed. At 16 knots, the Holtrop method produced a total resistance of 706.269 kN, the CFD simulation produced 655.434 kN for the initial model, and the Maxsurf Holtrop estimation produced 691.986 kN. The percentage difference between the Holtrop method and CFD was 7.76%, while the difference between Maxsurf Holtrop and CFD was 5.28% in magnitude. These results show that although the three methods produced different absolute resistance values, they followed a comparable resistance trend. Therefore, the comparison was used as a supporting consistency assessment, not as experimental validation.

Based on the CFD resistance results and the observed flow characteristics, Model C can be considered the most favourable hull configuration among the three tested models. However, this result should not be interpreted as a final or global hull-form optimization. The reduction in resistance is moderate, and the present study is limited to three hull variations evaluated through numerical simulations. In addition, only two angle modifications were considered, namely a 1° increase and a 1° decrease in the bow and stern line angles. Therefore, the findings should be regarded as a preliminary hydrodynamic assessment demonstrating that small changes in bow and stern line angles can influence the body-plan and sheer-plan geometry, affect flow development around the hull, and contribute to measurable changes in total resistance. Future studies may investigate a wider range of bow and stern line angle variations and incorporate experimental validation or towing-tank testing to further verify the numerical results.

CONCLUSION

This study demonstrates that bow and stern line angle variation influences the resistance performance of a 35,000 DWT bulk carrier, even when the principal dimensions of the vessel remain unchanged. The results indicate that the resistance difference among the tested models is associated with changes in the local hull-form transition, particularly in the bow entrance and stern run regions. Therefore, bow and stern line angle variation can be considered as one of the geometric parameters that affect hull resistance during the preliminary design stage. Among the three tested configurations, Model C was selected as the most favourable hull model because it produced the lowest total resistance at the operational speed of 16 knots. The reduction in resistance was not only shown by the numerical CFD results, but was also supported by the flow visualization. Model C showed a more controlled streamline pattern and smoother flow development around the hull compared with the other configurations. This indicates that reducing the bow and stern line angles by 1° may improve the local hull-form transition and reduce flow disturbance around the vessel.

The comparison among the Holtrop method, CFD simulation, and Maxsurf Holtrop estimation showed a similar increasing resistance trend with ship speed. This confirms that the CFD results follow a reasonable resistance tendency compared with empirical and software-based prediction methods. However, this comparison was used only as a consistency assessment of the resistance prediction trend and not as experimental validation.

Overall, the main finding of this study is that a small modification in the bow and stern line angles can affect the body-plan and sheer-plan geometry, influence flow development around the hull, and produce measurable changes in total resistance. Nevertheless, the resistance reduction obtained in Model C is moderate, so the result should be interpreted as a preliminary hydrodynamic assessment rather than a final hull-form optimization. Further studies involving broader angle variations, pressure-contour analysis, and experimental validation are recommended to strengthen the applicability of this hull-form modification.

ACKNOWLEDGEMENT

The authors would like to express their gratitude to the Ship Manufacturing Engineering Study Program, Department of Mechanical Engineering, Politeknik Negeri Banyuwangi, for the academic support provided during this research. The authors also appreciate the guidance and technical assistance received during data collection, hull modelling, and CFD simulation. These contributions supported the completion of this study.

REFERENCES

[1] K. Yeremenko, "International Maritime Organization and Decarbonization of Maritime Industry: Mandate and Instruments," *Lex Portus*, vol. 8, no. 3, Jul. 2022, doi: 10.26886/2524-101x.8.3.2022.2.

[2] F. Furcas, G. Vernengo, D. Villa, and S. Gaggero, "Design of Wake Equalizing Ducts using RANSE-based SBDO," *Applied Ocean Research*, vol. 97, p. 102087, Apr. 2020, doi: 10.1016/j.apor.2020.102087.

[3] Ang J.H., Goh C., Jirafe V.P., and Li Y., "International Conference on Computer Applications in Shipbuilding : (ICCAS 2017) : 26-28 September 2017, Singapore," in *RINA, Royal Institution of Naval Architects - International Conference on Computer Applications in Shipbuilding, ICCAS 2017*, Singapore: The Royal Institution of Naval Architects, 2017, pp. 77–86.

[4] R. Deng, S. Wang, Y. Hu, Y. Wang, and T. Wu, "The Effect of Hull Form Parameters on the Hydrodynamic Performance of a Bulk Carrier," *J. Mar. Sci. Eng.*, vol. 9, no. 4, p. 373, Apr. 2021, doi: 10.3390/jmse9040373.

[5] D. A. Hudson, A. F. Molland, and S. R. Turnock, *Ship Resistance and Propulsion : Practical Estimation of Propulsive Power*. Cambridge University Press, 2011.

[6] Y. K. Demirel, M. Khorasanchi, O. Turan, A. Incecik, and M. P. Schultz, "A CFD model for the frictional resistance prediction of antifouling coatings," *Ocean Engineering*, vol. 89, pp. 21–31, Oct. 2014, doi: 10.1016/j.oceaneng.2014.07.017.

[7] Moh. W. Wirawan, A. F. N. Oloan, A. G. Subakti, and J. R. Batosai, "CFD-Preliminary Design and Stability Analysis of a High-Speed Firefighting Boat for Remote Island Waterways," *Indonesian Journal of Maritime Technology*, vol. 2, no. 2, Dec. 2024, doi: 10.35718/ismatech.v2i2.1228.

[8] F. L. Dani, A. M. Raharja, H. M. Sihombing, and G. W. Abadi, "The Effect of Hard Chine Planing Variations on Resistance and Stability of a Patrol Boat Hull," *Indonesian Journal of Maritime Technology*, vol. 3, no. 2, Jan. 2026, doi: 10.35718/ismatech.v3i2.8481802.

[9] H. P. Nugroho, V. F. Syahputri, K. Anam, and M. A. Fadhilah, "A Hull Form Design Analysis with Variations of Block Coefficient (Cb) and Cross-Sectional Area (CSA)," *Indonesian Journal of Maritime Technology*, vol. 3, no. 2, Nov. 2025, doi: 10.35718/ismatech.v3i2.8481800.

[10] D. Eberechukwu Onwuegbuchunam, F. Chimobi Ogbenna, N. Charles Ezeanya and K. Okechukwu Okeke, "Ship Hull Form Optimization: A Computational Fluid Dynamics (CFD) Approach," *International Journal of Transportation Engineering and Technology*, vol. 5, no. 3, p. 43, 2019, doi: 10.11648/j.ijtet.20190503.11.

[11] M. Haase, G. Davidson, J. Binns, G. Thomas, and N. Bose, "Full-scale resistance prediction in finite waters: A study using computational fluid dynamics simulations, model test experiments and sea trial measurements," *Proceedings of the Institution of Mechanical Engineers, Part M: Journal of Engineering for the Maritime Environment*, vol. 231, no. 1, pp. 316–328, Feb. 2017, doi: 10.1177/1475090216642467.

[12] A. Miao, M. Zhao, and D. Wan, "CFD-based multi-objective optimisation of S60 Catamaran considering Demihull shape and separation," *Applied Ocean Research*, vol. 97, p. 102071, Apr. 2020, doi: 10.1016/j.apor.2020.102071.

[13] Achdri Fauzi Nugraha Oloan, Prabuditya Bhisma Wisnu Wardhana, Agung Fauzi Hanafi, and Yeddid Yonatan Eka Darma, "Influence of Ducted Propeller on Ro-Ro Vessels for Indonesia Inter-island Transportation," *International Journal of Maritime Engineering Innovation and Research*, vol. 10(4), pp. 1408–1415, Dec. 2025. doi: 10.12962/j25481479.v10i4.

[14] K. Takemura and H. Fujihisa, "High-pressure structural phase transition in indium," *Phys. Rev. B Condens. Matter*, vol. 47, no. 14, pp. 8465–8470, Apr. 1993, doi: 10.1103/physrevb. 47.8465.

[15] T. Tezdogan, Y. K. Demirel, P. Kellett, M. Khorasanchi, A. Incecik, and O. Turan, "Full-scale unsteady RANS CFD simulations of ship behaviour and performance in head seas due to slow steaming," *Ocean Engineering*, vol. 97, pp. 186–206, Mar. 2015, doi: 10.1016/j.oceaneng.2015.01.011.

[16] Yeddid Yonatan Eka Darma, Reyhan Arfananda Sugiarto, Achdri Fauzi Nugraha Oloan, and Fajri Narotama, "View of CFD-Based Comparative Study of Axe Bow and Bulbous Bow Designs for Corvette Warship Deployment in Natuna Waters," 2025. doi: 10.12962/j25481479.v10i3.

[17] Y. Yonatan, E. Darma, R. Hendra Pratama, I. G. N. A. Satria, P. Dharma Yudha, and A. I. Kusuma, "Impact of Stepped Hull Design on Speed Boat Performance: A CFD Study," 2024. doi: 10.5109/7236898.

[18] I. Martić, N. Degiuli, C. G. Grlj, K. Borčić, J. Andrišić, and I. Lalović, "Impact of the Longitudinal Center of Buoyancy on the Total Resistance of a Passenger Ship," *J. Mar. Sci. Eng.*, vol. 12, no. 10, p. 1749, Oct. 2024, doi: 10.3390/jmse12101749.

[19] E. Sugianto and A. Winarno, "Computational Ship Resistance Model to Determine the Power Requirements of A Bulk Carrier Ship 8664 DWT," *Marine Journal: Indonesian Journal of Marine Science and Technology*, vol. 10, no. 2, p. 168, Feb. 2018, doi: 10.21107/jk.v10i2.3411.

[20] Kurniawan T, Waskito, Achmad Hamman Gopar, Yanuar, and Gunawan, "Model-scale and full-scale Bulk Carrier ship resistance analysis using CFD simulations and empirical formulas," in *Prosiding SNTTM*, BKS-TM Indonesia, 2025, pp. 81–84. doi:10.71452/5fkat551.

[21] A. G. Elkafas, M. M. Elgohary, and A. E. Zeid, "Numerical study on the hydrodynamic drag force of a container ship model," *Alexandria Engineering Journal*, vol. 58, no. 3, pp. 849–859, Sep. 2019, doi: 10.1016/j.aej.2019.07.004.